J. Fluid Mech. (1990), *vol.* 214, *pp.* 437–454
Printed in Great Britain

On oscillatory flow over topography in a rotating fluid

By J. E. HART

Department of Astrophysical, Planetary and Atmospheric Sciences, Campus Box 391, University of Colorado, Boulder, CO 80309, USA

(Received 15 May 1989 and in revised form 29 September 1989)

Quasi-geostrophic β-plane motion of a homogeneous liquid over topography is considered for situations in which there is a time-periodic forcing of a zonal current. Such an oscillatory current generates a topographic Rossby wave response that has a complicated, but periodic, temporal structure. The linear solution shows resonances at all integer values of the β-parameter. The nonlinear analysis demonstrates that for weak friction and forcing, the resonances are bent and multiple equilibria of the time-dependent Rossby wave states are possible in certain parameter ranges. While the basic forced flow in the absence of topography has no time-mean, the nonlinear amplitude equations show that a mean retrograde (westward) Eulerian zonal flow is generated in the interactions of the forced flow with the topography. This result is in agreement with a previous theory of Samelson & Allen, constructed for strongly nonlinear flow over a series of asymptotically long ridges. However, in contrast to the behaviour of their amplitude equations for certain parameter settings, the near-resonant weakly nonlinear model for more or less isotropic bottom topography appears non-chaotic for all accessible parameter values.

1. Introduction

In the past few years there has been considerable interest in the influence of topography on large-scale flows in oceans and atmospheres. Using a truncated spectral model for barotropic quasi-geostrophic flow, Charney & DeVore (1979) predicted that steadily forced zonal flow over shallow mountains could exhibit multiple stationary equilibria. The existence of multiple states for constant external parameters had potential implications for the interpretation of phenomena like atmospheric blocking, and the bi-modality of atmospheric flow and the position of the Kuroshio current. The wave-mean interaction Charney–DeVore model was shown to overestimate the parameter space domain of multiple equilibria (Davey 1980*a*, *b*; Hart 1981), because when wave–wave interactions are included the strong wave–mean coupling required to get multiple states is reduced.

Two physical situations have been discussed where the original Charney–DeVore equations, or at least reduced versions of them with similar properties, appear as a rigorous asymptotic result. One case concerns zonal flow over a series of ridges with crests aligned perpendicular to the basic zonal current, and with slowly varying height in the cross-stream direction (Hart 1979). In the limit of very long ridges with close separations in the zonal direction, the wave–wave interactions scale out of the problem. The other asymptotic case deals with flow over more general topography, but with weak forcing, weak friction, and a zonal current that is near resonance (Pedlosky 1981). The imposed zonal flow velocity is nearly equal to the phase speed

of the topographically excited Rossby wave. In other words, the steady Rossby wave directly excited by the topography has the same spatial structure as a stationary free wave of the barotropic vorticity equation on a β-plane in the imposed steady zonal current. A finite-amplitude calculation then yields amplitude equations for the near-resonant mode which are identical in structure to those obtained by Charney & DeVore (1979), if the topographic amplitude is considered small in the latter work. All the above models for steady forcing have at least one stable fixed point, and extensive numerical calculations (Hart 1979) suggest that the steady Rossby wave solution(s) in the models are globally attracting. Thus there is no aperiodic time dependence of the predicted Eulerian fields.

Samelson & Allen (1987) were motivated by coastal oceanographic applications where there are fluctuating wind stresses to study a version of the Charney–DeVore model with time-periodic forcing. They envisioned a periodic alongshore current flowing over undulations in the continental shelf. Because of the well-known analogy between the planetary vorticity gradient β-effect and vortex stretching over a uniform topographic slope, their zonally invariant depth changes associated with the continental slope produce a model which is similar to that for planetary Rossby waves. Using the anisotropic topographic scaling of Hart (1979), they arrived at a low-dimensional model similar to that of Charney & DeVore but with a periodic forcing term. They found both periodic and chaotic solutions of their model equations, as well as regions where more than one attracting state exists. In addition, they showed that a purely periodic forcing leads to a time-mean Eulerian westward flow in the response. Such a mean flow has important consequences for tracer transport, for example, and its effect on Lagrangian particle paths can be significant.

Because of these results, we were motivated to attempt a laboratory experiment to investigate such processes further. To be practical, we had to consider more or less isotropic topography with similar cross-stream and zonal scales, rather than anisotropic ridges. The latter, in addition to being hard to construct, severely restrict parameter variations because of the requisite small lengthscale in the zonal direction for a laboratory apparatus of reasonable size. A topography with similar scales in both the downstream and the cross-stream directions is potentially more relevant to geophysical problems. As a first step, partially intended to aid in the interpretation of experimental results, we consider here the linear and weakly nonlinear theoretical problems of periodically forced flow over topography in a barotropic quasi-geostrophic fluid. The laboratory results will be reported in a future paper. The present work is organized as follows. After outlining the specific model, the forced linear problem, which has time-dependent coefficients, is solved exactly in §3. The linear solution shows that there will be resonances (an infinite response if friction is set to zero) at almost all integer values of the topographic β-parameter. The linear solution itself has a time mean, which also peaks at the resonances. To remove this resonance, and to consider how nonlinearity enters, we construct an asymptotic expansion for weak friction and forcing. This calculation is carried out in §4. A discussion of the results and a summary of the conclusions follow in §5.

2. Statement of the problem

The geometry of our problem is known in figure 1. We consider a one-layer constant-density flow in a cylinder of radius L. The fluid has a mean depth D and viscosity ν. The cylinder is rotated at a rate Ω which is made up of a large constant part Ω_0 and a periodic modulation with amplitude δ' and frequency ω. The rotation

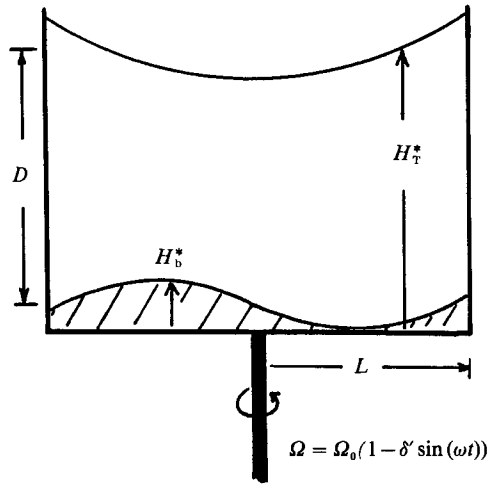

FIGURE 1. A cross-section of the flow. The rotation axis is oriented along the gravity vector and the upper surface is free.

rate is given by $\Omega = \Omega_0(1-\delta' \sin(\omega t))$, and we consider that $\delta' \ll 1$ and $\omega \ll \Omega_0$. This leads, as shown below, to quasi-geostrophic dynamics. In addition, it is assumed that the external Froude number

$$F_e = \frac{4\Omega_0^2 L^2}{gD},$$

with g being the gravitational acceleration, is small enough that the upper free surface undulations do not affect the internal dynamics. Formally this amounts to requiring that $F_e \ll \alpha_n^2$, where α_n is the total wavenumber of a topographically excited mode. In typical experiments $\alpha_2 = 5.13$ and F_e is less than 1, so this condition is satisfied. The theory is easily modified to take free-surface height fluctuations into account, but for simplicity we consider situations where the interface motions are small compared with both D and the topographic variations.

The bottom topography is given by a 'single-wave' structure

$$H_b^* = H_b J_n(\alpha_n r)\cos(n\theta), \tag{1}$$

where J_n is a Bessel function of index n, r is the non-dimensional radius (based on L), θ the azimuthal (zonal) angle, and α_n is the total wavenumber of the topography. It is assumed that $J_n(\alpha_n) = 0$ so that the topography vanishes at the outer sidewall. The philosophy is to study the response to flow over a single normal mode of the system and so the topography is chosen to be one of these modes. In a channel an equivalent topography would be $\sin(kx)\sin(ly)$, say. For the linear problem, a general topography can be constructed of a sum of Fourier–Bessel modes with terms like those in (1), and the response can be constructed by superimposing the individual responses. As far as the laboratory situation is concerned, having only one mode in H_b^* simplifies both the construction of the experiment and the interpretation of the data. Although the theoretical results are derived for cylindrical geometry, similar results will apply to channel flows. In the latter, n can be interpreted as the downstream wavenumber and the total wavenumber $\alpha_n^2 = m^2\pi^2 + n^2$ would explicitly contain the cross-stream wavenumber m. The only differences will be in the cross-stream structure of the disturbances in the channel as compared to those in a

cylinder, and, in particular, the values of the interaction integrals in table 1 will change.

When the tank rotates at an almost constant value of Ω the free surface deforms into a parabola given by

$$H_{\mathrm{T}}^{*} = \frac{\Omega^2 r^2 L^2}{2g}. \tag{2}$$

This parabolic distribution of height gives us an equivalent topographic β-effect.

Finally we consider the implications of the unique method of driving illustrated in figure 1. Our coordinates are imbedded in the cylinder so that the coordinate system is accelerating periodically. The Navier–Stokes equations of motion in this reference frame have the form

$$\frac{\partial \boldsymbol{v}}{\partial t} + \boldsymbol{v}\cdot\boldsymbol{\nabla v} + 2\boldsymbol{\Omega}\times\boldsymbol{v} = -\boldsymbol{\nabla} p + \nu\nabla^2\boldsymbol{v} + \boldsymbol{r}\times\frac{\mathrm{d}\boldsymbol{\Omega}}{\mathrm{d}t}. \tag{3}$$

Thus the modulation of the basic rotation produces a body force in the equations of motion. The curl of this body force is non-vanishing but constant in space so it excites a zonally invariant solid-body rotation in the frame of the cylinder. This solid rotation flow sloshes back and forth over the topography and provides the excitation of topographic Rossby waves in our experiments.

The Rossby number is defined here in terms of the forcing frequency ω,

$$\epsilon \equiv \frac{\omega}{2\Omega_0}, \tag{4}$$

relating the forcing frequency to the mean rotation rate. This number is assumed to be small. We also assume that δ', which can be thought of as a Rossby number based on the relative flow speed and cylinder radius, is small. The usual quasi-geostrophic barotropic vorticity equation can then be derived in situations where the topographic height variations are small with respect to D. Dissipation is provided by Ekman layer suction at the bottom (only). In this model we neglect the viscous sidewall and replace the formal outer ($r^* = L$) rigid boundary condition with an impermeable one. Such a replacement has only small effects in similar linear and finite-amplitude problems (Hart 1972).

If lengths are scaled with L, time with ω^{-1}, and velocity with ωL, then the depth-integrated (barotropic) vorticity equation written in terms of the geostrophic pressure is

$$\frac{\partial \nabla^2 P}{\partial t} + \mathrm{J}\left(P, \nabla^2 P + \frac{H_{\mathrm{b}}^{*} - H_{\mathrm{T}}^{*}}{\epsilon D}\right) + Q\nabla^2 P = -\frac{\hat{\boldsymbol{\Omega}}\cdot\boldsymbol{\nabla}\times\dfrac{\mathrm{d}\boldsymbol{\Omega}}{\mathrm{d}t}\times\boldsymbol{r}}{\omega^2}. \tag{5}$$

The velocities are given by geostrophic balance,

$$u = -\frac{\partial P}{r\partial\theta}, \quad v = \frac{\partial P}{\partial r}, \tag{6a}$$

and the Jacobian operator is

$$\mathrm{J}(A,B) \equiv \left(\frac{\partial A}{\partial r}\frac{\partial B}{r\partial\theta} - \frac{\partial B}{\partial r}\frac{\partial A}{r\partial\theta}\right). \tag{6b}$$

The friction parameter, which represents the ratio of the forcing period to the Ekman spin-down timescale, is defined by

$$Q = \frac{(\nu\Omega_0)^{\frac{1}{2}}}{\omega D}. \tag{7}$$

As stated above, when $\Omega = \Omega_0(1-\delta' \sin(\omega t))$ the forcing appears as a periodic vorticity source that is constant in space. This drives an axisymmetric solid-body rotation. If Q is small (values of 0.03 are typical in the laboratory) then the flow can be split up into a simple forced axisymmetric part and a topographically generated fluctuation. We write

$$P = \frac{\delta' r^2}{4\epsilon} \sin(t) + \phi(r, \theta, t). \tag{8}$$

If Q is not small we may rescale the amplitude and change the phase of the external modulation to give the first term on the right of (8). With this splitting the vorticity equation becomes

$$\frac{\partial \nabla^2 \phi}{\partial t} + \beta' \left(\frac{\partial \phi}{\partial \theta} + \eta' \sin(t) \frac{\partial \nabla^2 \phi}{\partial \theta} \right) + Q \nabla^2 \phi + S' \sin(t) \frac{\partial h_b}{\partial \theta} + \mathrm{J}(\phi, \nabla^2 \phi + \Gamma' h_b) = 0. \tag{9}$$

The parameters in this equation are

$$\beta' = \frac{H_T}{\epsilon D}, \quad \text{where } H_T = \frac{\Omega_0^2 L^2}{g}, \quad S' = \frac{\delta' H_b}{2\epsilon^2 D}, \tag{10a, b}$$

$$\eta' = \frac{\delta'}{2\epsilon\beta'}, \quad \Gamma' = \frac{H_b}{\epsilon D}, \tag{10c, d}$$

$$h_b = J_n(\alpha_n r) \cos(n\theta). \tag{10e}$$

The terms in (9) proportional to $\sin(t)$ represent forced advection of vorticity and forced flow over the zonally varying bottom topography, respectively.

Equation (9) is to be solved with no internal singularities, and with the geostrophic stream function ϕ being constant at $r = 1$. If (9) is integrated over the area inside the cylinder wall, a circulation condition at $r = 1$ is obtained (Hart 1979). The azimuthally averaged tangential velocity $\bar{v}(r = 1)$ in the ϕ-field decays to zero in a spindown time. We then require that $\bar{v}(r = 1) = 0$.

3. The linear solution

We first consider the forced linear equation obtained from (9) by setting the Jacobian term to zero. This is consistent when S' is very small. Assume a solution

$$\phi_1 = \mathrm{Re}\,(F(t)\,\mathrm{J}_n(\alpha_n r)\,\mathrm{e}^{\mathrm{i}n\theta}) \quad \text{with } \mathrm{J}_n(\alpha_n) = 0. \tag{11}$$

This leads to a first-order equation for the complex amplitude F which can be written as

$$\frac{\mathrm{d}F}{\mathrm{d}t} + QF - \mathrm{i}\beta F(1 - \eta \sin(t)) = \mathrm{i}S \sin(t), \tag{12}$$

where

$$S \equiv \frac{nS'}{\alpha_n^2}, \quad \eta' \equiv \eta \alpha_n^2, \quad \beta \equiv \frac{n\beta'}{\alpha_n^2}. \tag{13a–c}$$

The solution to (12) is obtained by writing

$$F = \mathrm{i}S\,\mathrm{e}^{-\chi(t)} G(t), \quad \chi(t) = \gamma t - \mathrm{i}\beta\eta \cos(t), \quad \gamma \equiv Q - \mathrm{i}\beta, \tag{14}$$

and finding that, for zero waves at $t = 0$,

$$G = \int_0^t \sin(t')\,\mathrm{e}^{\chi(t')}\,\mathrm{d}t'. \tag{15}$$

In evaluating this and other later integrals, considering $\exp(\text{const} \times \cos(t))$ as the generating function for the Bessel function I_ν is useful. The linear solution is found to be

$$F(t) \equiv X_c - \mathrm{i}X_s = -\frac{2S}{\beta\eta} \mathrm{e}^{\mathrm{i}\beta\eta\cos(t)} \sum_{k=1}^{\infty} k\, \mathrm{e}^{-\mathrm{i}\pi k/2} J_k(\beta\eta) \frac{\gamma \sin(kt) - k\cos(kt)}{k^2+\gamma^2}$$

$$-\frac{2S}{\beta\eta} \mathrm{e}^{-Qt} \mathrm{e}^{\mathrm{i}\beta\eta\cos(t)} \sum_{k=1}^{\infty} k\, \mathrm{e}^{-\mathrm{i}\pi k/2} J_k(\beta\eta) \frac{k\cos(kt)}{k^2+\gamma^2}. \tag{16}$$

The second summation, multiplied by $\exp(-Qt)$, is needed to satisfy a resting initial condition $F(0) = 0$. The influence of this initial condition decays away in a few spin-down times. In what follows we consider that the initial transients have decayed to inconsequential levels and consider only the first summation.

The solution (16) has some features in common with that for linear leewaves excited by oscillatory flow over topography in a non-rotating fluid (Bell 1975). One difference is that our problem explicitly contains frictional damping. Another especially interesting aspect of (16), not present in the lee-wave problem that is invariant to reflection of the zonal direction, is that $F(t)$ has a complex non-zero average for most parameter settings. Integrating over a cycle of the forcing and denoting this with an overbar gives

$$\bar{F} = \bar{X}_c - \mathrm{i}\bar{X}_s = \frac{2S}{\beta\eta} \sum_{k=1}^{\infty} \frac{k^2 (J_k(\beta\eta))^2}{k^2+\gamma^2}. \tag{17a}$$

It is useful to observe that

$$(k^2+\gamma^2)^{-1} = \frac{k^2-\beta^2+Q^2+2\mathrm{i}Q\beta}{(k^2-\beta^2)^2+2Q^2(k^2+\beta^2)+Q^4}, \tag{17b}$$

and that the parameter groups entering into (16) and (17a) are related to the topography and the Rossby numbers by

$$\frac{S}{\beta\eta} = \frac{H_\mathrm{b}}{\alpha_n^2 e}, \tag{17c}$$

and

$$\beta\eta = \frac{n\delta'}{2\epsilon}. \tag{17d}$$

Both the solution itself and the averages become very large for integer values of β. This resonance phenomenon is most prominent in the limit as $Q \to 0$. However, if $J_k(k\eta) \to 0$ at a resonant value $\beta = k = 1, 2, 3, \ldots$, then the flow will be small. The fact that the linear solution X_s has an average means that there is a topographic vortex, in the time-mean, which is not in phase with the topography. The essence of the dynamics, described above for arbitrary $\beta\eta$, can be illuminated by solving (12) using a regular perturbation in $\beta\eta \ll 1$ with $F = f_0 + \beta\eta f_1 + \ldots$. It is readily shown that the solution at order $(\beta\eta)^0$, which is not periodically advected by the basic sloshing flow at this level, is given the purely sinusoidal form

$$f_0 = \frac{S(\gamma\sin(t) - \mathrm{i}\cos(t))}{1-\gamma^2}.$$

The flow generated by the periodic solid rotation flowing back and forth over the topography has an in-phase and an out-of-phase component. Both components feel the bottom friction and so are multiplied by the complex number $(1-\gamma^2)^{-1}$, for non-

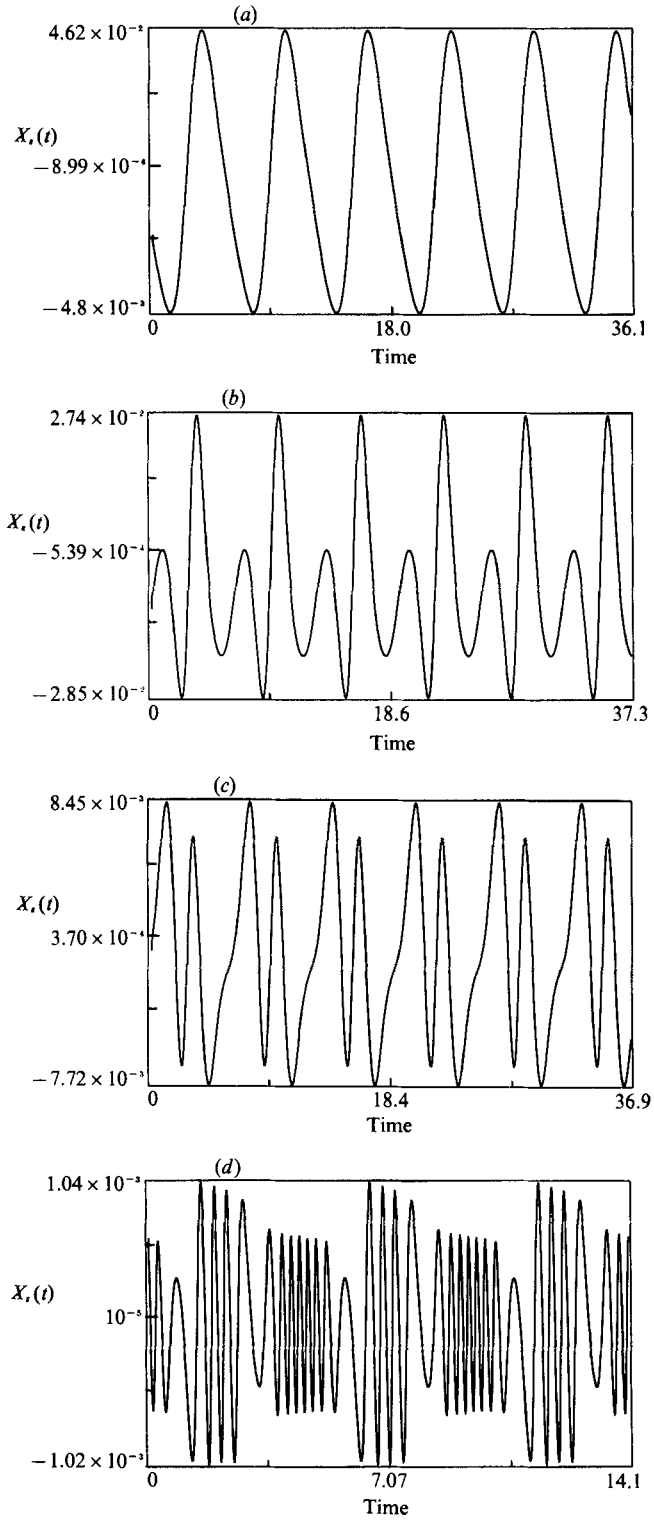

FIGURE 2. Time series from the linear solution for X_s. All have $Q = 0.04$, $S = 0.01$. (*a*) $\beta = 0.9$, $\eta = 0.5$, (*b*) $\beta = 0.9$, $\eta = 2.0$, (*c*) $\beta = 2.3$, $\eta = 0.5$, (*d*) $\beta = 0.4$, $\eta = 5$.

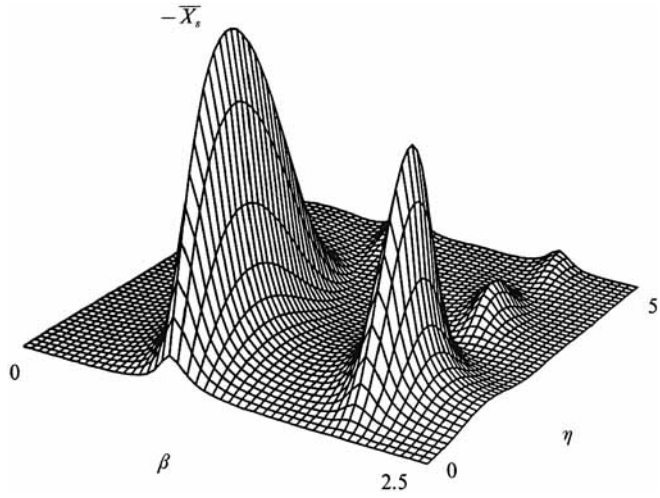

FIGURE 3. The solution surface giving $-\bar{X}_s$ from (16) as a function of β and η for $Q = 0.1$, $S = 0.1$. The maximum value is 0.209 and the minimum value is 0.

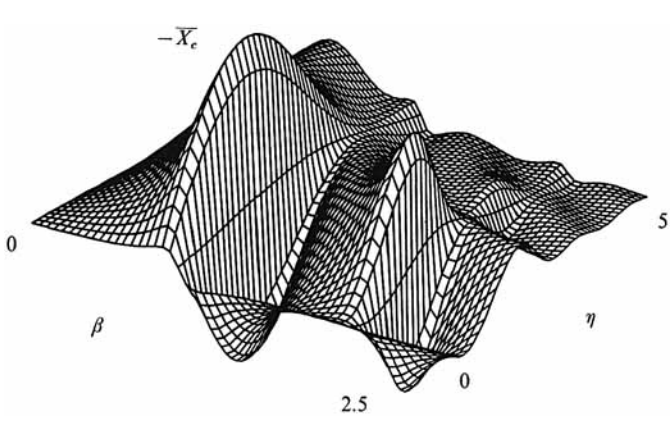

FIGURE 4. The solution surface for $\bar{X}_c$ from (16) as in figure 3. The maximum value is 0.124 and the minimum value is -0.087.

zero Q. The order-$\beta\eta$ correction f_1 is generated by vorticity advection of the sinusoidally varying mountain vortices by the basic sloshing:

$$\frac{\mathrm{d}f_1}{\mathrm{d}t} + \gamma f_1 = -\sin(t) f_0 = -\frac{S(\gamma \sin^2(t) - 0.5\mathrm{i} \sin(2t))}{1-\gamma^2}.$$

Integrating this over a period shows that the stationary mountain-induced vortex is just

$$\bar{f}_1 = -\frac{S}{2(1-\gamma^2)}.$$

The imaginary component of $\bar{f}_1$, which represents the amplitude of the $J_2 \sin(n\theta)$ part of the flow phase-shifted westward from the topographic crests, is proportional to the friction parameter Q (see (17b) with $k = 1$). This is the part of the total geostrophic pressure field which has its highs correlated with the mountain upslopes. The resulting form drag is responsible for the zonally invariant retrograde mean flow generation described in the following section. There is a balance between mean flow

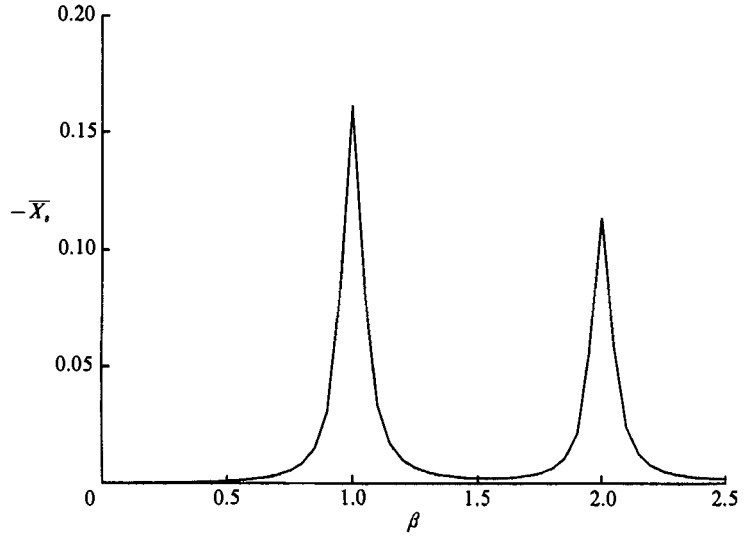

FIGURE 5. A cut through figure 3 at $\eta = 1.0$. The resonances are centred at integer values of β.

generation by form drag and mean flow damping by bottom friction. Both are linear in Q. Thus the resulting zonal jets are dependent on friction for their existence, but their dynamics will be independent of its magnitude, except at resonance where $\bar{X}_s$ is proportional to Q^{-1}.

Although the topographically forced Rossby wave has a simple spatial structure, its time dependence can be very complicated. For near integer values of β the summations in (16) and (17) will be dominated by a single term which has a frequency reflecting that particular $k = \beta$. However, even in this limit the exponential expression outside the summation can generate a contribution to the frequency spectrum that is multi-spiked and significant when $\beta\eta$ is not small (e.g. when the frequency Rossby number ϵ and the flow-speed Rossby number δ' are comparable).

Figure 2 shows several example time series of X_s for typical laboratory values of Q (the solution scales linearly with S). When β is near a resonant value and η is small the solution is almost monochromatic. However when β is off-resonance, many terms in the sum contribute to F and the response involves higher-frequency harmonics. The same is true when β is near-resonant but η is large. If β is non-resonant and η is large the flows can become quite complex (figure 2*d*) with highly structured waveforms contained within each forcing cycle. Simple single-harmonic flow oscillations over topography can, evidently, generate quite complicated Eulerian time histories.

Figures 3 and 4 show how the averaged values of X_s and X_c depend on β and η for a particular value of Q. Changing Q alters the sharpness of the ridges but not their locations. If one is looking for large mean flows, then one needs to pick η and β so that β is near a resonant integer k and $\beta\eta$ is near a maximum of $J_k(\beta\eta)$.

In the linear version of the problem the slopes of figure 3 are not folded over. This is illustrated in figure 5. The behaviour near $\beta = k$ is symmetric so that there is only one $\bar{X}_s$ for each value of β. We expect that if friction is small, nonlinearity will be important and may bend the resonance. If the bending is strong enough, then there will be multiple amplitudes of the averaged fields (and of F itself) for fixed external parameters.

4. Finite-amplitude analysis

In order to investigate resonance bending as well as the nonlinear evolution of such forced flows, we consider a near-resonant expansion. The analysis parallels that of Pedlovsky (1981) for the steadily forced problem. The idea is to consider what happens at small friction when β is near k. Then there will be a single dominant component of the linear solution $F(t)$ which is the resonant one. Since this mode is much larger than all the other non-resonant harmonics, we consider it by itself and ask how its evolution is affected by both the weak friction and by nonlinear interactions. To carry out the analysis we write

$$\phi = \sigma\phi_1 + \sigma^2\phi_2 + \sigma^3\phi_3 + \ldots, \tag{18}$$

where

$$\sigma \equiv S^{\frac{1}{3}} \ll 1,$$

and S is taken to be positive without loss of generality.

The β parameter is assumed to be near-resonant so that

$$\beta = j + \Delta,$$

where j is an integer and Δ is small number of order σ^2. The other parameters are chosen so that Q and Γ are both of order σ^2. Time is split into a fast time (order one) and a slow time $\tau = \sigma^2 t$. Thus the time derivative transforms as

$$\frac{\partial}{\partial t} \to \frac{\partial}{\partial t} + \sigma^2 \frac{\partial}{\partial \tau}.$$

Inserting the expansion (18) into (9) and using this ordering yields a sequence of problems, the solution of which will give the long-time evolutionary behaviour of the near-resonant mode. At order σ we get the linear but inviscid problem:

$$\frac{\partial \nabla^2\phi_1}{\partial t} + \beta' \frac{\partial \phi_1}{\partial \theta} + \beta'\eta \sin(t) \frac{\partial \nabla^2 \phi_1}{\partial \theta} = 0. \tag{19}$$

The solution for the resonant mode is

$$\phi_1 = \mathrm{Re}\,(A(\tau)\, \mathrm{e}^{\mathrm{i}\chi(t)} J_n(\alpha_n r)). \tag{20a}$$

From here on

$$\chi \equiv \beta\tau + \beta\eta \cos(t) + n\theta. \tag{20b}$$

The goal of the finite-amplitude analysis is to determine $A(\tau)$. At $O(\sigma^2)$ the vorticity equation is identical to (19) except that ϕ_1 is replaced by ϕ_2. This is because $\mathrm{J}(\phi_1, \nabla^2\phi_1) \equiv 0$ and the topography, which is proportional to $S = \sigma^3$ has not entered the problem at this level. The solution again includes the resonant mode, which can be renormalized into ϕ_1 and thus is not explicitly carried in the calculation. In addition there is the possibility of a slow-time-varying zonal flow. Thus, we take

$$\phi_2 = \Phi_2(r, \tau). \tag{21}$$

The zonal flow correction (modifying the original fast-periodic part in (8)) is not yet determined.

The order-σ^3 equation is

$$\frac{\partial \nabla^2\phi_3}{\partial t} + \beta' \frac{\partial \phi_3}{\partial \theta} + \beta\eta \sin(t) \frac{\partial \nabla^2 \phi_3}{\partial \theta} = -\frac{\partial \nabla^2 \phi_1}{\partial \tau} - \frac{Q}{\sigma^2} \nabla^2 \phi_1 - \alpha_n^2 \frac{\Delta}{n\sigma^2} \frac{\partial \phi_1}{\partial \theta}$$
$$- \frac{S'}{\sigma^3} \sin(t) \frac{\partial h_b}{\partial \theta} + \frac{1}{r}\left[\frac{\partial \phi_1}{\partial \theta} \frac{\partial \nabla_0^2 \Phi_2}{\partial r} - \frac{\partial \Phi_2}{\partial r} \frac{\partial \nabla^2 \phi_1}{\partial \theta}\right]. \tag{22}$$

When all terms on the right-hand side of (22) that project onto the free solution (20) are removed, the amplitude equation of the slow variation of A with τ is obtained. Operationally we pick off all modes on the right-hand side with $\exp(\mathrm{i}\chi(t,\theta))$ dependence. The right-hand side of (22) is multiplied by $\exp(-\mathrm{i}\chi(t,\theta))$, the adjoint time and θ-function to the homogeneous solution (20), and integrate over a cycle in t and in θ. To obtain the projection onto the spatial structure of the resonant mode, the terms remaining are multiplied by $rJ_n(\alpha_n r)$ and integrated over radius. The amplitude equation that results represents the removal of secular resonances in the expansion. It is

$$\frac{\mathrm{d}A}{\mathrm{d}\tau}+\frac{Q}{\sigma^2}A-\frac{\mathrm{i}\Delta}{S^{\frac{1}{2}}}A+\frac{2\mathrm{i}nA}{\alpha_n^2 J_{n-1}^2(\alpha_n)}\int_0^1\left(J_n^2(\alpha_n r)\left(\frac{\partial\nabla^2\Phi_2}{\partial r}+\alpha_n^2\frac{\partial\Phi_2}{\partial r}\right)\right)\mathrm{d}r=\mathrm{i}I_j, \tag{23a}$$

where

$$I_j\equiv \mathrm{e}^{\mathrm{i}\pi j/2}\frac{J_j(j\eta)}{\eta}. \tag{23b}$$

In order to close (23) an equation for the mean flow correction Φ_2 is needed. This function changes only in r and τ and it can only be determined at order σ^4. The mean flow is altered by vorticity advections, topographic interactions and friction according to

$$\frac{\partial\nabla^2\Phi_2}{\partial\tau}+\frac{Q}{\sigma^2}\nabla^2\Phi_2=-\bar{\mathrm{J}}\left(\phi_1,\nabla^2\phi_3+\frac{\Gamma}{\sigma^2}h\right)-\bar{\mathrm{J}}(\phi_3,\nabla^2\phi_1). \tag{24}$$

Here the overbar denotes a time average over a cycle in t, and an average around θ in azimuth. As shown in Pedlosky (1981), it is not necessary to explicitly calculate ϕ_3 in order to evaluate the right-hand side of (24). Integrations by parts in the θ-average gives

$$\frac{\partial\nabla^2\Phi_2}{\partial\tau}+\frac{Q}{\sigma^2}\nabla^2\Phi_2=\frac{1}{r}\frac{\partial}{\partial r}\overline{\left(\frac{\partial\phi_1}{\partial\theta}\left(\nabla^2\phi_3+\frac{\Gamma}{\sigma^2}h\right)\right)}. \tag{25}$$

We now substitute for $\phi_{1\theta}$ from (19). Further integrations by parts in θ and t lead to

$$\frac{\partial\nabla^2\Phi_2}{\partial\tau}+\frac{Q}{\sigma^2}\nabla^2\Phi_2=-\frac{1}{r}\frac{\partial}{\partial r}\overline{\left(\phi_1\left(\nabla^2\phi_{3t}+\beta'\phi_{3\theta}+\beta'\eta'\sin(t)\,\nabla^2\phi_{3\theta}-\frac{\Gamma}{\sigma^2}h\theta\right)\right)}. \tag{26}$$

Now (22) can be used directly to show that

$$\frac{\partial\nabla^2\Phi_2}{\partial\tau}+\frac{Q}{\sigma^2}\nabla^2\Phi_2=-n\alpha_n^2\frac{\partial}{r\,\partial r}J_n^2(\alpha_n r)\left(\frac{\mathrm{d}|A|^2}{\mathrm{d}\tau}+\frac{2Q}{\sigma^2}|A|^2\right)$$

$$=-n\alpha_n^2\frac{\partial}{r\,\partial r}J_n^2(\alpha_n r)\,2\,\mathrm{Im}\,(AI_j^*), \tag{27}$$

where the last step is via application of (23). Finally we notice that the $\Phi_2(r,\tau)$-field separates in radius and time. Define $M(t)$ by

$$\frac{\partial\Phi_2}{\partial r}=v_2=\frac{2n}{r}\alpha_n^2 J_n^2(\alpha_n r)M(\tau). \tag{28}$$

The slow-time zonal current v_2 has a broad jet-like profile in radius with no flow reversals, as shown in figure 6. Multiple jets, all in the same direction, are found if α_n corresponds to a second or higher root of $J_n(\alpha_n)=0$. It will turn out that M is steady on the slow-time so (28) means that there is a constant azimuthally invariant current generated by the Rossby waves sloshing back and forth over the topography.

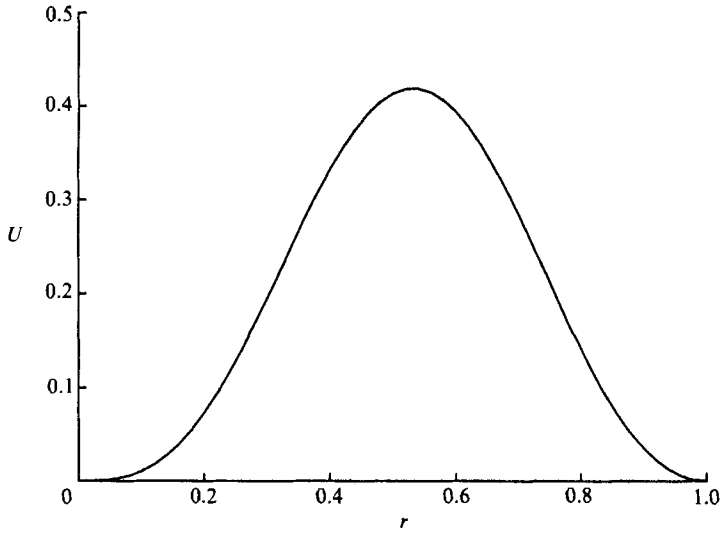

FIGURE 6. The time and zonally averaged flow velocity profile. The ordinate shows $J_n^2(\alpha_n r)/r$ for $n = 2$.

The integrals in (23) are now carried out using the r-functions in (28). We make one last transformation:

$$A = I_j q^{-\frac{1}{3}}(X_c - \mathrm{i}X_s), \quad M = |I_j|^2 q^{-\frac{2}{3}} U(t), \quad \tau' = q^{\frac{1}{3}}\tau,$$

where

$$q \equiv b_n |I_j|^2,$$

and

$$b_n = 4n^2\alpha_n \frac{2}{J_{n-1}^2(\alpha_n)} \int_0^1 r^{-1}(J_n^4(\alpha_n r) - 4J_n^2(\alpha_n r) J_n'^2(\alpha_n r))\,\mathrm{d}r.$$

This yields the final amplitude equations for the long-time evolution of the near-resonant mode:

$$\left(\frac{\mathrm{d}}{\mathrm{d}\tau'} + \mu\right) U(\tau') = X_s, \tag{29}$$

$$\left(\frac{\mathrm{d}}{\mathrm{d}\tau'} + \mu\right) X_c(\tau') = (\delta - U) X_s, \tag{30}$$

$$\left(\frac{\mathrm{d}}{\mathrm{d}\tau'} + \mu\right) X_s(\tau') = -(\delta - U) X_c - 1, \tag{31}$$

where

$$\mu \equiv \frac{Q}{\sigma^2 q^{\frac{1}{3}}} = \frac{Q}{S^{\frac{2}{3}}(b_n |I_j|^2)^{\frac{1}{3}}}, \tag{32}$$

and

$$\delta \equiv \frac{\Delta}{\sigma^2 q^{\frac{1}{3}}} = \frac{\Delta}{S^{\frac{2}{3}}(b_n |I_j|^2)^{\frac{1}{3}}}. \tag{33}$$

The definition of δ should not be confused with that used in (8).

The values of b_n have been tabulated for several values of n using a single humped radial distribution of topography. The results are shown in table 1.

The amplitude equations (29)–(31) are identical in form to those of Pedlosky (1981) for stationary Rossby waves. His equations in turn are the same as the anisotropic mountain equations of Hart (1979) when the forcing is near resonant and small in the

n	α_n	b_n
1	3.832	−11.6
2	5.136	13.7
3	6.380	100.4
4	7.588	225.9

TABLE 1. Wave-mean interaction integrals

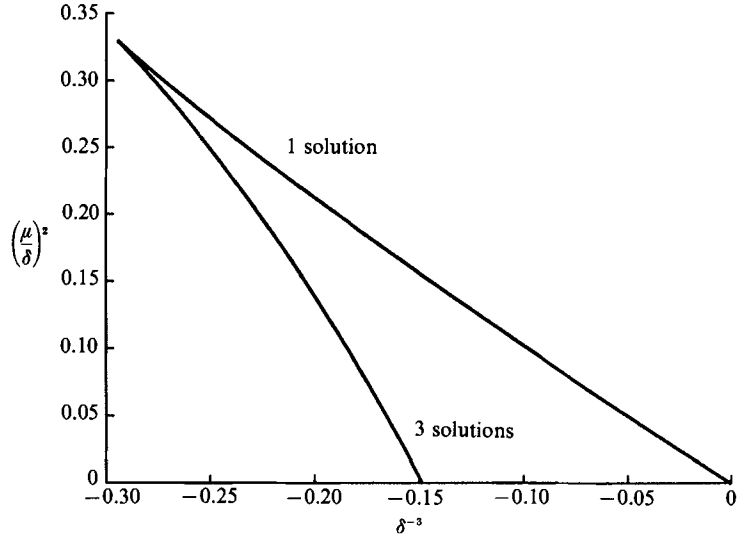

FIGURE 7. The region of parameter space where multiple real and steady solutions of the nonlinear amplitude equation are found.

latter. Notice that in contrast with the Samelson & Allen nonlinear amplitude equations, there is no periodic forcing in (29)–(31). All the fast-time dependence is here contained in the linear solution. One result of this is that there is apparently no chaotic behaviour in the present model. The scaling is such that the fast-time zonal flows, $\Phi_3(r,t)$ and higher orders, do not enter into a determination of the amplitude equations. It is when these fast-time zonal currents are significant that chaotic motions in the Eulerian fields become possible.

Numerical integrations of (29)–(31) indicate that solutions always proceed to a stable steady state. These steady solutions are given, as in Pedlosky (1981), by the real roots of

$$\mu^2 U + (\delta - U)^2 U + 1 = 0. \tag{34}$$

Since this is a cubic, there are either one or three real roots. Equation (34) shows that when a real root exists it must be negative. Applying the standard condition for the existence of all real roots to a cubic polynomial with real coefficients gives a simple delineation of the parameter space occupied by multiple steady states. For (34) this condition for multiple real roots reduces to

$$\frac{3\mu^2}{\delta^2} - 1 + \left(1 + \frac{9\mu^2}{\delta^2} + \frac{27}{2\delta^3}\right)^2 < 0. \tag{35}$$

Equating this expression to zero and solving for δ^{-3} as a function of $\mu^2\delta^{-2}$ gives the range of δ for multiple roots for any $\mu^2\delta^{-2}$ less than one third. The formula is

$$\delta^{-3} = -\frac{2}{27}\left[1 + \frac{9\mu^2}{\delta^2} \pm \left(1 - \frac{3\mu^2}{\delta^2}\right)^{\frac{1}{2}}\right]. \tag{36}$$

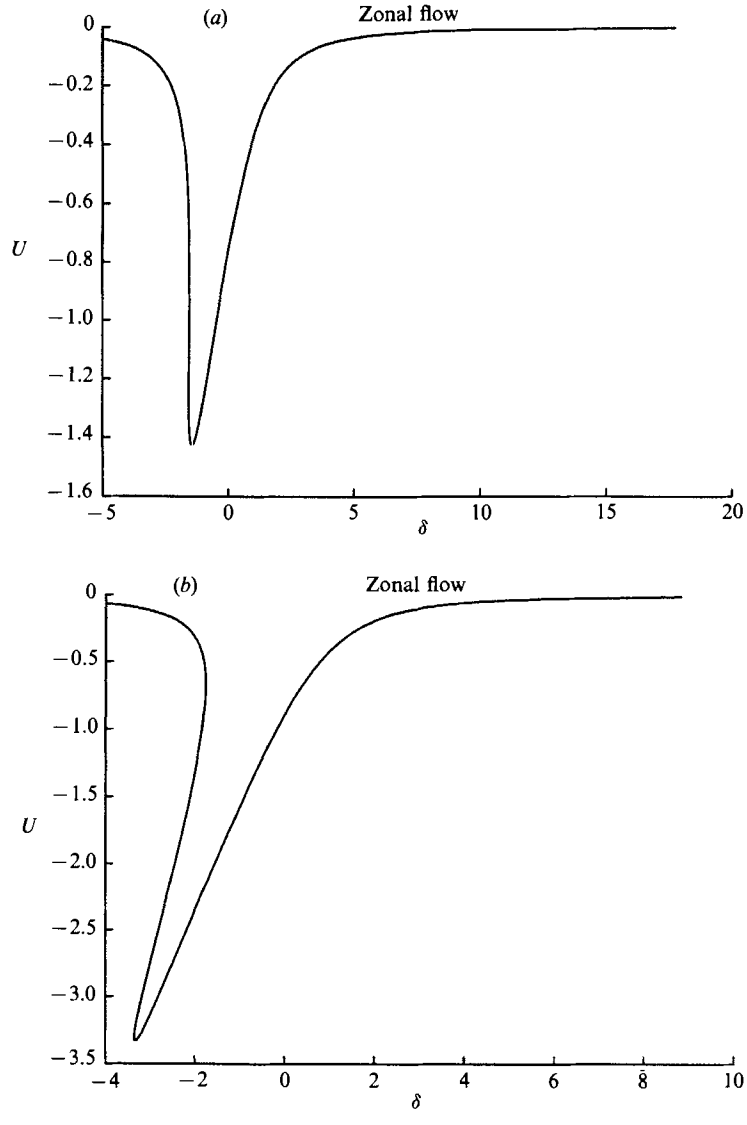

FIGURE 8. Typical distributions of U with δ. (a) $\mu^2 = 0.7$, (β) $\mu^2 = 0.3$.

The curves are plotted in figure 7. The diagram is best interpreted as giving the range in μ over which multiple roots occur for each δ. Only negative and somewhat substantial δ values give multiple roots. This means that the sign of Δb_n must be negative. The system must be below resonance (or subresonant) for $n > 1$, but must be super resonant ($\Delta > 0$) for $n = 1$. It will be more difficult to make δ large at large n, because the b_n are larger. Also, as S is made larger, the region of multiple equilibria will occur at larger Δ, that is farther from linear frequency resonance.

Figure 8 shows the steady solutions U for two values of μ^2. Looked at upside down, they illustrate the bending of the resonance discussed earlier. In figure 8 (a), for each value of δ, μ^2 is too large to fall within the 3-solution region of figure 7 and only one U exists. When μ^2 decreases to 0.3 for a range of δ the tipping or folding of the valley

creates three possible U values. It is easy to show that the inner root is linearly unstable.

From (34) it is seen that the maximum amplitude of the retrograde mean current is obtained when $\delta = -\mu^{-2}$, and has a value $U = -\mu^{-2}$. This relationship giving the biggest possible mean zonal velocity translates into

$$\Delta_{\max} = -\frac{b_n J_j^2(j\eta) S^2}{\eta^2 Q^2}, \tag{37}$$

suggesting that large mean Eulerian currents would be obtained on the subresonant side of the jth resonances for $n > 1$. In a typical case where η is order one and S is not too much less than Q, the large values of b_n indicate that the shift away from the linear resonance case can be substantial and increases rapidly with the bottom topography amplitude. This type of behaviour is exactly what we find in the laboratory (J. M. Pratte & J. E. Hart, in preparation).

5. Conclusions

A sinusoidal oscillatory zonal flow over topography generates a topographic Rossby wave field. If there is no advection by the oscillatory current, only vortex stretching, then a pure single-frequency motion ensues. Vortices are alternately generated by planetary vortex compression and expansion in a symmetric manner. There is no net mean flow generation. However, when advection of the wave field by the oscillatory basic current is taken into account ($\eta > 0$), the periodic advection coupled with the natural westward propagation of Rossby waves leads to an asymmetry that can generate a stationary component to the linear solution. When friction is present, the stationary field has a component with anticyclones (high pressures) on the westward sides of the crests. This generates a wave drag which causes a retrograde (westward) mean flow generation. The wave amplitude and mean flow generation is friction-limited near resonance in the linear problem. Resonances occur when the natural frequency of a Rossby wave with an azimuthal wavenumber n and total wavenumber α (contained in the bottom topography spectrum) is equal to an integer multiple of the forcing frequency ω.

The weakly nonlinear analysis showed that the resonances are bent to the subcritical side when $n > 1$. That is, the larger wave responses to the applied forcing should appear at forcing frequencies ω lower than that required for resonance. Hysteresis and multiple solutions with different periodic and steady components are also predicted. In the weak friction limit these multiple states for fixed external parameters occur when $Q^2\Delta^{-2}$ is less than one third and $S^2 b_n |I_j|^2 \Delta^{-3}$ falls into a fairly narrow range of possible values between 0 and -0.3 whose width depends on the smallness of $Q^2\Delta^{-2}$ (figure 7). No chaotic behaviour has been found in extensive numerical integrations of the model studied here. Orbits always fall onto one or more of the attracting fixed points of equations (29)–(31).

As with any linear or weakly nonlinear model, it is appropriate to ask questions about the range of validity. How small must σ be for the analysis to work? For finite σ (i.e. finite topography), are the predicted retrograde flows suppressed by nonlinearities and wave interactions scaled out of the analysis? Can one observe the complex time dependencies suggested by the linear theory in a real physical system? Current laboratory experiments indicate that the multichromatic time series and subresonant mean flow maxima predicted for $n = 2$ topography indeed occur.

However, good quantitative agreement between theory and experiment for modest topography features of order 10% of the fluid depth requires modifications to the present theory.

Compared with the Samelson–Allen model of oscillatory flow over topography, the present Eulerian fields are rather tame. After initial transients die out, the solutions are periodic in time, never chaotic. Eulerian chaos may appear at large topographic amplitudes not covered by our model, but the relaxation of the anisotropic mountain limit for *weak* forcing appears to lead to a system with no chaos. On the other hand, the Lagrangian trajectories in our model are much more complicated and chaotic than those found in the anisotropic mountain model when the Eulerian fields in both cases are periodic. The trajectories of fluid columns are given by the Hamiltonian system

$$\frac{\mathrm{d}r}{\mathrm{d}t} = u = -\frac{1}{r}\frac{\partial P(r,\theta,t)}{\partial \theta}, \tag{38}$$

$$\frac{r\,\mathrm{d}\theta}{\mathrm{d}t} = v = \frac{\partial P(r,\theta,t)}{\partial r}, \tag{39}$$

where the total stream function P serves as the Hamiltonian. In the anisotropic mountain limit the azimuthal angular velocity v/r is independent of r so that (39) can be integrated (for periodic v/r) by itself. Once $\theta(t)$ is a known periodic function, (38) can be integrated as a one-dimensional dynamical system with time-periodic coefficients. Because the phase-space dimension of this latter problem is two (r and the phase of time), the resulting particle paths are not chaotic.

In our problem there is no such simplification. The Hamiltonian trajectory equations are obtained using (8), (18), (21) and (28). For wavenumber $n = 2$ fields they are

$$\frac{\mathrm{d}r}{\mathrm{d}t} = -\frac{2\sigma}{r} J_2(\alpha_2 r)\,\mathrm{Re}\,(A\,\mathrm{i}\,\mathrm{e}^{\mathrm{i}t+2\theta+\beta\eta\cos(t)}), \tag{40}$$

$$\frac{\mathrm{d}\theta}{\mathrm{d}t} = \frac{\delta'}{2\epsilon}\sin(t) + \frac{\sigma\,\partial J_2(\alpha_2 r)}{r\,\partial r}\mathrm{Re}\,(\mathrm{A}\,\mathrm{e}^{\mathrm{i}t+2\theta+\beta\eta\cos(t)}) + \frac{\sigma^2}{r^2}4\alpha_2^2(\alpha_2 r)M, \tag{41}$$

where the steady values of A and M are retrieved from (34), (29)–(31) and the transformations following (28). Equations (40) and (41) are not integrable when σ is non-zero. Numerical experiments predict chaotic wanderings of surface floats through the (r,θ)-phase space with velocities that in some circumstances far exceed those associated with the back-and-forth oscillations of the reference frame. Mixing regions near separatrix crossings are found, along with invariant tori, as expected from KAM theory.

Figure 9 illustrates the typical phenomena. We consider $n = 2$ so that $b_n = 13.7$, $A_{\mathrm{r}} = 0.42U$, $A_{\mathrm{i}} = 0.42\mu^{-1}(\delta - U)U$, and $M = 0.17U$. From figure 8(b) with $\mu^2 = 0.3$ we take $\delta = -3$ so that there are two stable solutions for the mean flow, $U = -0.116$ and $U = -3.13$. The former is typical of an off-resonant weak retrograde jet, while the latter represents the near-resonant situation with a strong mean flow. We now vary $\sigma = S^{\frac{1}{3}}$ and note that with μ and δ fixed this corresponds to simultaneous variations in the friction parameter $Q = 1/3\sigma^2$ and the detuning parameter $\Delta = -7.14\sigma^2$. Figure 9 shows stroboscopic sections for various σ. These sections are constructed by plotting particle positions at fixed phases of time, here either $t = 2 + 2j\pi$ or just $t = 2j\pi$ (in figure 9d) for $j = 0, 1, \ldots, 300$. First look at the strong jet case with $U = -3.13$. At very small σ the motion is regular almost everywhere (figure 9a), the exception being very near a separatrix crossing at the origin. As δ increases (figures 9b, 9c, 9e)

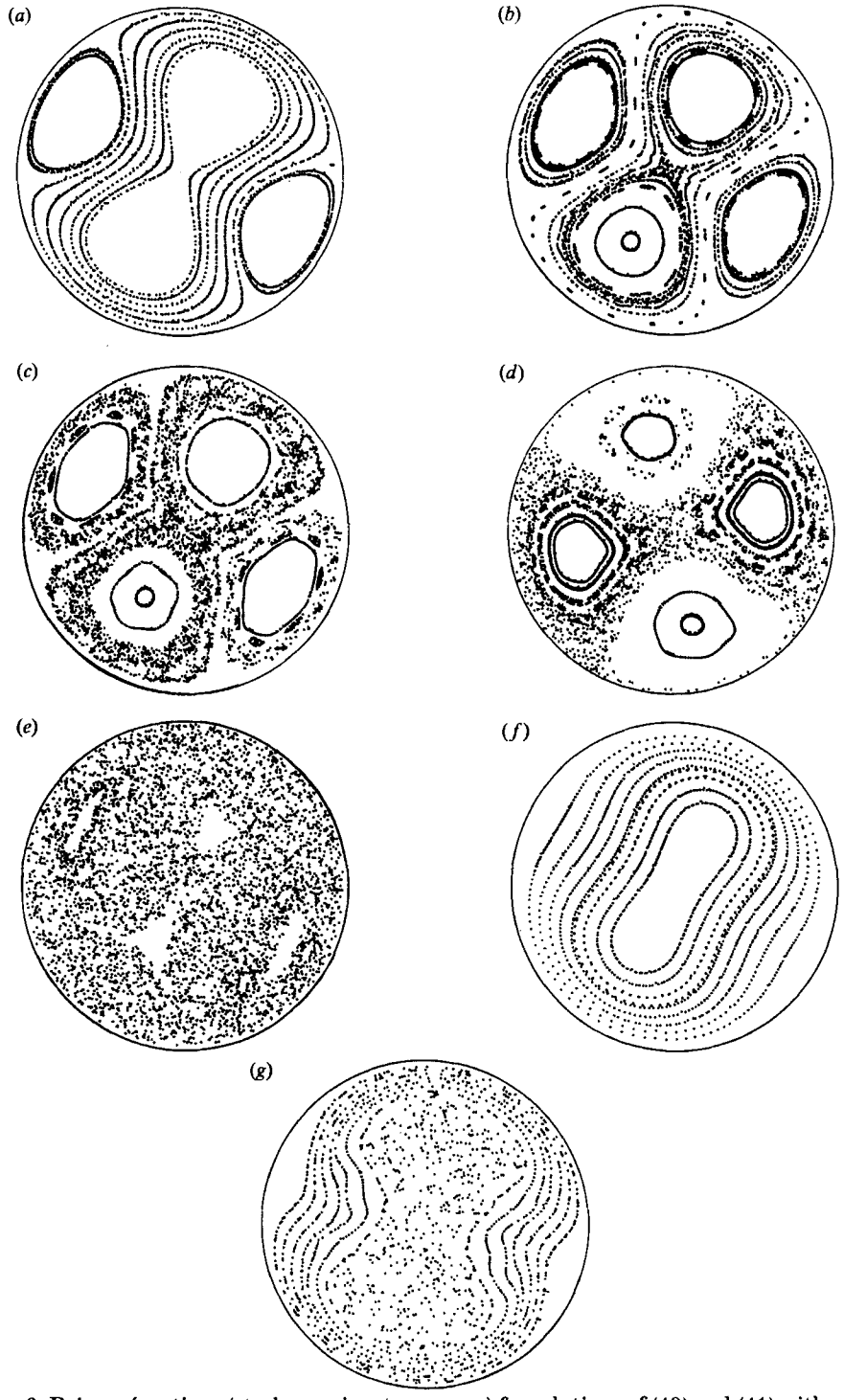

FIGURE 9. Poincaré sections (stroboscopic return maps) for solutions of (40) and (41) with a number of initial particle positions. Three o'clock defines $\theta = 0$ and $n = 2$ (see (1)). All have $\delta'/2\epsilon = 0.5$, $\beta\eta = \delta' n/2\epsilon = 1.0$, and trigger phase angle 2.0 (except *d*, which has phase 0). Cases (*a–e*) have $U = -3.13$ and (*f–g*) have $U = -0.116$. (*a*) $\sigma = 0.005$, (*b*) $\sigma = 0.015$, (*c*, *d*) $\sigma = 0.02$, (*e*, *f*) $\sigma = 0.04$, (*g*) $\sigma = 0.4$.

chaotic behaviour associated with the four hyperbolic fixed points of the map located at the wall gradually merges with that near the origin to fill almost all of the space inside the cylinder except that occupied by four small regular islands (figure 9*e*). When a different phase angle for the section is chosen (figure 9*d*) the plot rotates and also changes its structure slightly because time shifts in (40) and (41) are not simply equivalent to rotations in angle.

For the large-U solution, chaotic particle paths dominate when σ is greater than about 0.03. The associated value of S is miniscule ($\approx 3 \times 10^{-5}$), so this model predicts chaotic Lagrangian trajectories for all but the smallest mountains. For the off-resonant solution, $U = -0.116$, shown in figures 9(*f*) and 9(*g*), σ must be considerably larger before the KAM tori are almost all destroyed. In this example $\sigma > 0.4$, or $S > 0.06$, are required, values which tax the validity of the weakly nonlinear expansion. At fixed σ there is a substantial qualitative difference in the particle tracks between the two multiple states (compare figures 9*e* and 9*f*).

The strong flows (near resonance), complicated but periodic Eulerian time dependence, and chaotic Lagrangian motions in this simple system may have important ramifications for problems such as the interaction of time-dependent eddies with smaller scale bottom topography, periodic wind-forced currents, and seasonally forced flows in gyres like the western Indian ocean. We have concentrated here on quasi-geostrophic flow with a sinusoidal forcing. Questions such as the response in the presence of vertical stratification and to ageostrophic forcing where ϵ and/or δ' are not small remain to be studied.

The author thanks the National Science Foundation for support of this research under grants ATM 86-12736 and ATM 88-20430 to the University of Colorado. Computing support was provided through NASA contract NAS8-31958. He also thanks John Allen for helpful discussions which provided a stimulus for this work, and Scott Jones for suggesting the computation of the Poincaré sections for the Lagrangian trajectories.

REFERENCES

Bell, T. H. 1975 Lee waves in stratified flow with simple harmonic time dependence. *J. Fluid Mech.* **67**, 705–722.

Charney, J. G. & DeVore, J. G. 1979 Multiple flow equilibria in the atmosphere and blocking. *J. Atmos. Sci.* **36**, 1205–1216.

Davey, M. K. 1980*a* A quasi-linear theory for rotating flow over topography. Part 1. Steady β-plane channel. *J. Fluid Mech.* **99**, 267–292.

Davey, M. K. 1980*b* A quasi-linear theory for rotating flow over topography. Part 2. β-plane annulus. *J. Fluid Mech.* **103**, 297–320.

Hart, J. E. 1972 A laboratory study of baroclinic instability. *Geophys. Fluid Dyn.* **3**, 181–209.

Hart, J. E. 1979 Barotropic quasi-geostrophic flow over anisotropic mountains: multi-equilibria and bifurcations. *J. Atmos. Sci.* **36**, 1736–1746.

Hart, J. E. 1981 Experiments on rapidly rotating recycling flow over topography. *Tellus* **33**, 597–603.

Pedlosky, J. 1981 Resonant topographic waves in barotropic and baroclinic flows. *J. Atmos. Sci.* **12**, 2626–2641.

Samelson, R. M. & Allen J. S. 1987 Quasi-geostrophic topographically generated mean flow over a continental margin. *J. Phys. Oceanogr.*, **17**, 2043–2064.